

PARACHUTES

A Computer Program for Calculating Ram-Air Parachutes

Theory Document

**E. Ortega
R. Flores**

PARACHUTES

A Computer Program for Calculating Ram-Air Parachutes

Theory Document

E. Ortega
R. Flores

Publication CIMNE N^o-415, September 2016

Summary

PARACHUTES is a computer program developed at the International Center for Numerical Methods in Engineering (CIMNE) for the simulation of ram-air (gliding) parachute systems. The solution methodology in PARACHUTES is based on two unsteady calculation modules which work in a coupled manner. The aerodynamics of the gliding parachute is solved by a low-order panel method and a finite-element technique is used for the structure. The latter allows modelling the suspension lines, textile fabric and suspended payloads of a typical parachute system by means of cable, membrane and solid linear elements. For specified flight conditions, the simulation program solves the fluid-structural problem governing the behavior of arbitrary parachute-payload configurations and also allows analyzing user-defined maneuvers. This document describes the theoretical formulation and the numerical procedures adopted in PARACHUTES.

Table of Contents

1	Introduction.....	3
2	Overview of PARACHUTES.....	4
2.1	Structural modelling.....	4
2.2	Aerodynamic modelling.....	5
3	PARACHUTES theoretical background and implementation	7
3.1	The structural model.....	7
3.1.1	Finite element discretization.....	7
3.1.2	Time integration.....	8
3.1.3	Numerical damping.....	8
3.1.3.1	Setting Rayleigh damping parameters.....	10
3.1.3.2	Absolute and relative damping.....	11
3.1.4	Element formulation.....	11
3.1.4.1	Two-node linear cable element.....	11
3.1.4.2	Three-node linear membrane element.....	12
3.1.4.3	Four-node linear tetrahedral solid element.....	17
3.1.5	Additional features.....	22
3.1.5.1	Rigid body modelling.....	22
3.1.5.2	Internal computation of the cable drag forces.....	23
3.1.5.3	Control over changes in cable length.....	24
3.2	The aerodynamic model.....	24
3.2.1	Numerical solution of the potential flow problem.....	27
3.2.1.1	Calculation of the influence coefficients.....	29
3.2.1.2	Velocity potential influence coefficients.....	30
3.2.1.3	Velocity vector influence coefficients.....	31
3.2.2	Wake treatment.....	32
3.2.3	Computation of aerodynamic loads.....	32
3.2.4	Treatment of the canopy internal flow.....	33
3.2.5	Robustness control.....	34
3.3	The coupling methodology.....	35
3.3.1	Apparent-mass effects.....	36
3.4	Computational performance.....	36
4	PARACHUTES graphical user interface.....	37
5	Conclusions.....	37
	References.....	37

1 Introduction

The numerical simulation of parachutes is an active research line at the International Center for Numerical Methods in Engineering (CIMNE), and several analysis tools have been developed to tackle these problems over the last years. At present, CIMNE has gained experience in the field of parachute simulation, mainly throughout a consecution of research projects such as PARACIMSA [1] and PARAPLANE [2, 3], both developed in cooperation with CIMSA Ingeniería en Sistemas [4], a leading parachute designer and manufacturer company.

The computer program PARACHUTES is intended for the unsteady simulation of ram-air (gliding) parachutes and general payloads and interface systems. This program is the result of the evolution of a previous code called PARACIMSA. The latter, which was based on an aerodynamic stationary panel method coupled with an implicit finite element (FE) technique for solving the structure, had a two-fold purpose: the prediction of the loads acting on the structure of ram-air parachutes and the approximate treatment of manoeuvres. PARACIMSA has been satisfactorily applied to a variety of parachute models and flight conditions; however, certain lack of robustness reported by the users (mainly due to the implicit structural technique adopted) and the need to broaden the range of applications (in order to deal with full unsteady problems) called for upgrading. In view of the changes and improvements required, the need to adopt a different approach in order to improve and extend the capabilities of the simulation code was evident. Thus, the development of a new simulation program was undertaken based on the experience gained in all the previous work, and putting special emphasis on robustness and computational efficiency. The main objective is to obtain a practical tool for the design, evaluation and analysis of gliding parachute-payload systems.

The computer program PARACHUTES is designed to address these requirements. It solves the aerodynamic and structural problems governing the behavior of the parachute-payload system in a coupled manner. The solver consists of two unsteady calculation modules, aerodynamic and structural, which are sequentially advanced in time in an explicit manner exchanging data at each time step (2-way staggered coupling). The aerodynamics is solved with a low-order panel method and a FE technique is used for the structure. The latter allows modelling the suspension lines, textile fabric and suspended payloads of a typical parachute system by means of cable, membrane and solid linear elements. The theoretical formulation and numerical implementation used in PARACHUTES are described in detail in this document.

This report is organized as follows. Section 2 presents an overview of the solution procedure adopted in PARACHUTES. The theoretical formulation and the solution strategy developed for the structural and aerodynamic calculation modules are described in Section 3. Details about

the coupling procedure and computer requirements are also given in the same section. The graphical user interface developed to facilitate the use of the PARACHUTES is referenced in Section 4. Finally, current and future developments are outlined in Section 5.

2 Overview of PARACHUTES

The requirements that should meet a simulation program intended for the practical analysis of parachute-payload systems are very challenging for several reasons. From the structural point of view, the parachutes are complex in design and behavior. Braced membranes, such as parachute canopies, cannot equilibrate an arbitrary set of loads unless drastic geometrical changes take place; thus, the structural response is extremely nonlinear. The lack of bending stiffness of the structural components makes them buckle (wrinkle) under compressive loads, exhibiting an asymmetric behavior. The flow surrounding the parachute is also complex and usually highly unsteady. The aerodynamic model adopted should deal with the geometrical changes experienced by the structure, and also take into account the presence of large unsteady wakes and aerodynamic interactions between the different parts of the parachute. The numerical tools designed for practical analysis of parachute-payload configurations should have enough capability to deal with this complex behavior with reliability and a reasonable computational cost.

In order to address these challenges, the choice of the structural and aerodynamic solvers (and the coupling methodology) was thoroughly examined in PARACHUTES from two different points of view. First, the capabilities of the available techniques to deal with the typical situations encountered during the flight of gliding parachutes; second, their robustness and chances of achieving low computational costs through efficient numerical implementations. An overview of the structural and aerodynamic models is presented next.

2.1 Structural modelling

In order to model the structural behavior of the parachute-payload system it was decided to use a FE explicit dynamic solver. An unsteady analysis is not affected by the problems caused by the lack of a definite static equilibrium configuration and the solution is always unique (the structure is constantly in equilibrium with the inertial forces). Even when only the long-term static response is sought, the dynamic approach offers some advantages. Furthermore, the extension to transient dynamic problems becomes trivial. In view of the expected difficulties, an explicit time integration scheme was adopted. Although explicit methods are conditionally stable (the stability limit is determined by the material properties and the model geometry) the cost per time step is low. Moreover, the explicit method is extremely insensitive to highly

nonlinear structural behavior and requires a number of time steps that does not change substantially as the system response becomes more complex. Material nonlinearities and large displacements, which are detrimental for the convergence of an implicit scheme, do not affect adversely the explicit method. A further benefit is the fact that the algorithm can be easily vectorized, so important speed-ups can be achieved on parallel computers. Concerning the modelling of the structural components of the parachute-payload system, linear cable and membrane elements are implemented for the suspension lines and the textile fabric, respectively. In addition, solid elements are used for the payloads suspended from the parachute. Inside each element a simple small-strain formulation is used. Tensile deformations are always small, and even when compressive strains become large due to the inclusion of a wrinkling model (zero compression stiffness for cable and membrane elements), there is no stress associated and, correspondingly, no strain energy. Hence, the small-strain formulation is adequate since only tensile deformations are needed to calculate the stress state.

In addition to the mentioned structural elements, PARACHUTES also offers the possibility to account for rigid bodies. This is very useful for the treatment of suspended payloads. Since the deformation of the latter are usually negligible, these can be considered rigid and a large computational saving can be obtained. A rigid body has only 6 degrees of freedom and it has no upper bound on its allowable time step; therefore, it can be included in the model at virtually no extra cost. The strategy in PARACHUTES is to convert arbitrary element sets (of cable, membrane or solid type) into a single (or various) rigid body, whose motion is fully characterized by its orientation and the position of its center of mass. By using rigid elements the dynamics of the system can be solved with accuracy in a much more efficient manner.

The structural solver has other functionalities of interests for the designer, for example the possibility to prescribe changes in the cable length to simulate manoeuvres. To this end, the required deformation of the parachute steering lines must be entered in tabular form, with a set of time-deformation values. During the simulation, the solver applies the prescribed deformation, interpolating between the input values to guarantee smooth variations.

2.2 Aerodynamic modelling

In spite of the fact that the structural solution approach described above is general and can be applied to any kind of parachute-payload configuration, the higher computational cost of a general flow solution was not considered cost-effective in the context of the present development. Therefore, a potential flow model was adopted, reducing the scope of the aerodynamic solution. Note that this simplified flow model is deemed acceptable for the

simulation of gliding parachutes because normally no extensive flow separation regions are present during its operation. Moreover, the modular approach adopted for the code allows to enhance the flow solver (for instance through semi-empirical corrections, boundary layer models, etc.) to adapt it to problems going beyond the scope of potential methods.

In order to solve the potential problem, an unsteady low-order panel method was selected. The use of a low-order method (where the singularities have constant strength over the panels) is justified because its reported accuracy is nearly similar to that of higher-order methods [5] (linear or quadratics), and also have substantial robustness, lower complexity and computational cost. Furthermore, low-order methods do not require exact matching between the panels, which considerably simplifies the discretization. In order to model the wake, a simple time-stepping method is used. In this method, the wake develops from specified shedding lines along the body according to both, the motion of the latter and the total velocity induced at the panels (wake rollup). The wake doublet strength of the panels shed into the wake is determined by enforcing the Kutta condition at the shedding lines, thus no additional unknowns are introduced into the problem. In addition, the time-stepping methodology allows for a natural development of the wake and is simpler and less expensive than other techniques used for example in steady state methods, which requires wake relaxation iterations in a fictitious time to obtain the proper wake shape (e.g. [6]).

The wind loads acting on the cables (i.e. suspension and control lines) are treated in PARACHUTES in a simplified manner. The chords are considered as long circular cylinders exposed to the wind, and proper experimental drag coefficients must be specified to compute the aerodynamic loads. Furthermore, it is also possible to use aerodynamic force functions to account for the wind loads acting on solid suspended bodies (e.g. payloads). These functions can be obtained from experimental data fitting, in terms of the body shape and attitude. The simplified treatment of the aerodynamic loads on the payloads and suspension lines enhances significantly the modelling capabilities of the simulation code with a negligible additional cost.

Finally, PARACHUTES also accounts for apparent mass effects. This additional mass due to the inertia of the air surrounding the structure can affect the transient behaviour and stability of very light structures (such as the parachute canopy) and should be accounted for, particularly in transient problems. To this end, the model of Lissaman and Brown [7] is used.

3 PARACHUTES theoretical background and implementation

The theoretical formulation employed in PARACHUTES is described in this section. Details of the coupling methodology and the numerical implementation are also given. Further information can be found in [8, 9] and [10].

3.1 The structural model

The starting point for solving the structural problem is the virtual work principle. It states that when the system is in equilibrium the change in strain energy caused by an arbitrary virtual displacement field equals the work done by the external forces. This leads to

$$\sum_{i,j} \int_{\Omega} \sigma_{ij} \delta \varepsilon_{ij} d\Omega = \sum_i \int_{\Omega} b_i \delta u_i d\Omega + \sum_i \int_{\Gamma_N} \bar{t}_i \delta u_i d\Gamma \quad (1)$$

where \bar{t}_i stands for prescribed surface traction on the boundary Γ_N , σ_{ij} denotes the components of the stress tensor and $\delta \varepsilon_{ij}$ is the virtual strain corresponding to the virtual displacement field δu_{ij} . In dynamic problems, the body forces (b_i) includes the inertial loads

$$b_i|_{inertial} = -\rho \frac{d^2 u_i}{dt^2} \quad (2)$$

where ρ is the density of the solid.

3.1.1 Finite element discretization

In order to obtain a discretized form of Eq. (1), an approximate FE solution is built by interpolating the nodal values of the displacements [11], i.e.

$$\tilde{u}_i(\mathbf{x}) = N^k(\mathbf{x}) \tilde{u}_i^k \quad (3)$$

being \tilde{u}_i^k the approximate solution corresponding to the k^{th} node of an element and N^k the interpolation (shape) function. Supra-indexes indicate nodal values, and summation is assumed over the repeated index k . Introducing the interpolated displacement field into Eq. (1) and taking into account that the virtual nodal displacements are arbitrary, the following discretized system of equations is obtained

$$\mathbf{M}\ddot{\mathbf{u}} = \mathbf{b} + \mathbf{t} - \mathbf{I} \quad (4)$$

where \mathbf{M} is the mass matrix of the system, \mathbf{b} and \mathbf{t} represent the external nodal generalized forces and \mathbf{I} is the internal force vector. After giving proper initial conditions,

$$\mathbf{u}|_{t=0} = \mathbf{u}_0 \quad \text{and} \quad \dot{\mathbf{u}}|_{t=0} = \dot{\mathbf{u}}_0 \quad (5)$$

the system of ordinary differential equations (4) can be advanced in time to yield the displacement field at every instant time. To speed up the computations, the mass matrix \mathbf{M} is replaced by its lumped (diagonal) counterpart \mathbf{M}^d [12] without significant loss of accuracy.

3.1.2 Time integration

In order to advance in time the system of equations (4), an explicit second-order central differencing scheme is selected due to its high efficiency and acceptable accuracy [13]. Given a series of points in time $t^{(i)}$, the change in midpoint velocity can be defined as

$$\frac{d\mathbf{u}^{(i+1/2)}}{dt} - \frac{d\mathbf{u}^{(i-1/2)}}{dt} = \frac{\Delta t^{(i+1)} + \Delta t^{(i)}}{2} \cdot \frac{d^2\mathbf{u}^{(i)}}{dt^2} \quad (6)$$

where $\Delta t^{(i)} = t^{(i)} - t^{(i-1)}$. Once the intermediate velocities have been computed, the displacements can be updated according to

$$\mathbf{u}^{(i+1)} = \mathbf{u}^{(i)} + \Delta t^{(i+1)} \cdot \frac{d\mathbf{u}^{(i+1/2)}}{dt} = \mathbf{u}^{(i)} + \Delta t^{(i+1)} \cdot \left[\frac{d\mathbf{u}^{(i-1/2)}}{dt} + \frac{\Delta t^{(i+1)} + \Delta t^{(i)}}{2} \cdot \frac{d^2\mathbf{u}^{(i)}}{dt^2} \right] \quad (7)$$

The method outlined has a very low computational cost per time step but it is only conditionally stable. This means the time increment must be limited in order to prevent divergence of the solution. The maximum allowable time step is given by

$$\Delta t \leq \frac{2}{\omega_{\max}} \quad (8)$$

with ω_{\max} being the angular frequency of the highest eigenmode of the system. An alternative estimate of the maximum time step is given by the minimum transit time of the dilatational waves across the elements of the mesh, i.e.

$$\Delta t \leq \min \left(\frac{L_e}{c_d} \right) \quad (9)$$

where L_e is a characteristic element dimension and c_d is the dilatational wave speed.

3.1.3 Numerical damping

The second-order central difference scheme adopted above has very low numerical damping. Therefore, any spurious oscillation introduced into the system persists for a long time (e.g. the perturbations due to a sudden change in the applied load when the aerodynamic solver advances one time step). This can lead to noisy solutions, either slowing down the convergence to steady-state or contaminating the response of the system in transient

simulations. In order to overcome these problems it is advisable to introduce some form of numerical damping into the equations. Two forms of user-adjustable damping are included in PARACHUTES to improve the control over the solution process: Rayleigh damping and bulk viscosity. In the former, the damping matrix is built from the mass and stiffness matrices of the system [12] as follows

$$\mathbf{C} = \alpha \mathbf{M} + \beta \mathbf{K} \quad (10)$$

and the system of equations (4) supplemented with this damping term becomes

$$\mathbf{M}\ddot{\mathbf{u}} = \mathbf{b} + \mathbf{t} - \mathbf{I} - \mathbf{C}\dot{\mathbf{u}} \quad (11)$$

From Eqs. (10) and (11) it is observed that the α -term creates a damping force which is proportional to the mass of the nodes (mass-proportional damping) and its absolute velocity. This is roughly equivalent to having the nodes of the structure moving through a viscous fluid. The damping ratio introduced by the mass-proportional damping on a mode of frequency ω is

$$\xi = \frac{\alpha}{2\omega} \quad (12)$$

Hence, it is apparent from Eq. (12) that the α -term affects mainly the low frequency components of the solution. For transient simulations the parameter α should be set to zero (or to a very small value) to avoid contamination of the dynamic response. On the other hand, when only the long-term response is sought, the mass-proportional damping can be used to accelerate the convergence to a steady-state solution.

The β -term in Eq. (10) introduces forces that are proportional to the material strain rate (stiffness-proportional damping). This is implemented adding an extra stress $\boldsymbol{\sigma}_d$ to the constitutive law. This is given by

$$\boldsymbol{\sigma}_d = \beta \mathbf{D}^{el} : \dot{\boldsymbol{\epsilon}} \quad (13)$$

where \mathbf{D}^{el} is the tangent stiffness tensor of the material. The fraction of critical damping for a given mode is (only the high order modes are affected appreciably)

$$\xi = \frac{\beta \omega}{2} \quad (14)$$

Typically, high order modes are involved in small patches of elements that do not contribute appreciably to the overall system response, but can introduce unwanted noise in the solution. When stiffness proportional damping is introduced, the stability limit (9) is reduced to

$$\Delta t \leq \frac{2}{\omega_{\max}} \left(\sqrt{1 + \xi_{\max}^2} - \xi_{\max} \right) \quad \text{where} \quad \xi_{\max} = \frac{\beta \omega_{\max}}{2} \quad (15)$$

Additionally to Rayleigh damping, a bulk viscosity term is also included in PARACHUTES. This prevents high frequency ringing caused by excitation of the element dilatational modes, which are always associated with the highest eigenvalues of the system. To this end, an additional hydrostatic stress proportional to the volumetric strain rate is introduced in the constitutive routines. This is given by

$$\sigma_h = b \rho c_d L_e \dot{\epsilon}_{vol} \quad (16)$$

The parameter b in Eq. (16) controls the amount of damping applied to the dilatational mode; satisfactory results are obtained setting $b=0.06-0.1$.

3.1.3.1 Setting Rayleigh damping parameters

While there is no universal value suitable for all problems, there is a simple method to estimate the value required for each particular case. Concerning the parameter α , the procedure consists on running a few iterations of the solver to determine the lowest frequency (ω_{min}) of the oscillations present. It always corresponds to the global behavior of the system (i.e. a rigid body-like motion such as pitch, roll or yaw). If fast convergence to the steady state is sought, the damping ratio of the lowest mode should be close to one. To this effect, α is set to

$$\alpha = 2\theta\omega_{min} \quad (0 < \theta < 1) \quad (17)$$

and the parameter θ is used to ensure that the amount of damping is subcritical (supercritical damping should be avoided as it would slow down convergence to the steady state). A reasonable choice is $\theta \approx 0.3$. In many typical parachute applications the period of the global motion is on the order of one second. Therefore, the order of magnitude of the mass-proportional damping parameter is 1Hz.

Regarding the stiffness-proportional damping, a similar analysis can be performed to adjust the parameter β . Note that since the latter affects the stability limit, it is necessary to prevent a significant decrease of the time increment, which would increase the computational cost. To this end, it is reasonable to set $\xi_{max} \approx 2\%$, and an appropriate value for β is

$$\beta \approx \frac{0.05}{\omega_{max}} \quad (18)$$

Note that the damping ratio of the highest modes need not be large as they undergo many oscillations during the simulation. Therefore, their amplitude decreases very quickly.

3.1.3.2 Absolute and relative damping

As seen in Eq. (11), the dissipation or viscous forces introduced by the contribution of the mass and stiffness damping are proportional to the absolute velocity of the nodes. Therefore, these forces can greatly affect the behavior of structures that undergo significant rigid body motion. In order to minimize this undesirable effect (particularly for the α -term which affects the lower modes), PARACHUTES has the ability to compute the dissipation force using velocities relative to the center of mass of the system. In this way, only the displacements (or vibration) relative to the global motion of the structure are damped. This also makes that the dissipation forces act in a local manner and tend to zero when the steady state is achieved. The use of relative damping allows increasing the value of the damping parameters without significantly affecting the global behaviour of the system.

3.1.4 Element formulation

Linear two-node cables, three-node membranes and four-node tetrahedral solid elements are employed in PARACHUTES. As an introduction to the details of implementation, the cable element formulation is described first. Due to the fact that only small tensile strains are expected, a small-strain formulation has been adopted to calculate the elemental stresses. This assumption allows for efficient coding while maintaining acceptable accuracy.

3.1.4.1 Two-node linear cable element

Let us consider a linear cable element stretching between nodes i and j , having cross sectional area A and subject to a distributed loading per unit length \mathbf{f}_d as shown in Figure 1.

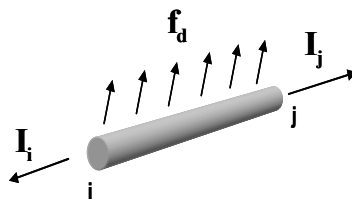


Figure 1. Linear cable element subject to internal and external loads.

As large displacements are expected, the position of the nodes can be written either on the undeformed (reference) configuration or in the deformed (current) configuration. From now on upper-case letters will denote the original coordinates while lower-case will be reserved for the current configuration. For example, the original length of the cable element is given by

$$L_0 = \|\mathbf{X}_j - \mathbf{X}_i\| \quad (19)$$

while the actual length at any given time is

$$L(t) = \|\mathbf{x}_j - \mathbf{x}_i\| \quad (20)$$

From the change in length of the element the axial strain and stress can be obtained. Assuming linear elastic behavior

$$\varepsilon = \frac{L - L_0}{L_0} ; \quad \sigma = \max(0, E\varepsilon) \quad (21)$$

The cables buckle instantly under compressive loads, thus, a lower bound of zero is enforced in Eq. (21) and the corresponding magnitude of the internal nodal forces is $l_i = \sigma A$. No distinction is made between the reference (A_0) and the updated cross-section (A). When the element is active (under tension) the strains are always small so either value is acceptable.

The nodal generalized external force due to a distributed loading acting on the element (e.g. due to wind loads) can be computed by

$$\mathbf{b}_i = \int_0^L N_i \mathbf{f}_d dL = \frac{L}{2} \mathbf{f}_d \quad (22)$$

where it is assumed that \mathbf{f}_d remains constant across the element.

In many occasions the CAD geometry available does not reflect the nominal (i.e. in-flight) length of the suspension lines, and these should be adjusted to obtain the correct response of the system. In particular, this is quite common for the steering lines that the pilot must pull once the canopy is deployed. In addition, further changes in the cable lengths can be required to simulate maneuvers or to achieve a desired flight configuration. In any case, the required control inputs can be reproduced either using a combination of sliding cable elements and prescribed displacements or, in a much simpler way, by changing the undeformed cable length. The second approach is followed in PARACHUTES. Hence, the code allows the user to change the L_0 value in Eq. (21) as the simulation progresses. The time evolution of L_0 for the relevant elements can be specified as part of the input file (see Section 3.1.5.3).

3.1.4.2 Three-node linear membrane element

A triangular element with three vertices x^1 , x^2 and x^3 is defined according to Figure 2. Given that large displacements are expected, the strain state of the element is easier to evaluate in a local corrotational frame than in the global reference system [14].

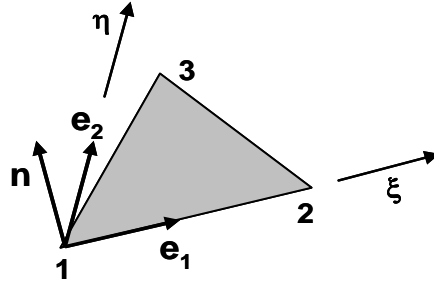


Figure 2. Linear membrane element corrotational local frame.

The three unit vectors along the local axes can be obtained from

$$\mathbf{e}_1 = \frac{\mathbf{x}^2 - \mathbf{x}^1}{\|\mathbf{x}^2 - \mathbf{x}^1\|} ; \quad \mathbf{n} = \frac{\mathbf{e}_1 \times (\mathbf{x}^3 - \mathbf{x}^1)}{\|\mathbf{e}_1 \times (\mathbf{x}^3 - \mathbf{x}^1)\|} ; \quad \mathbf{e}_2 = \mathbf{n} \times \mathbf{e}_1 \quad (23)$$

Thus, any point of the triangle can now be identified by its two local coordinates (ξ, η)

$$(\xi, \eta) = ((\mathbf{x} - \mathbf{x}^1) \cdot \mathbf{e}_1, (\mathbf{x} - \mathbf{x}^1) \cdot \mathbf{e}_2) \quad (24)$$

As a linear triangle always remains flat, the problem is greatly simplified by analyzing the stress state on the ξ - η plane (see Figure 3).

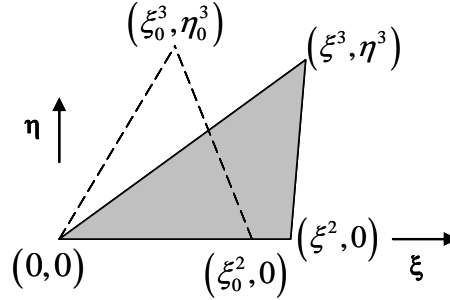


Figure 3. Nodal coordinates in the triangle local reference frame.

The components of the strain tensor can be determined using the gradients of the element shape functions as follows

$$\begin{bmatrix} \varepsilon_\xi \\ \varepsilon_\eta \\ \gamma_{\xi\eta} \end{bmatrix} = \begin{bmatrix} \frac{\partial N^1}{\partial \xi} & 0 & \frac{\partial N^2}{\partial \xi} & 0 & 0 & 0 \\ 0 & \frac{\partial N^1}{\partial \eta} & 0 & \frac{\partial N^2}{\partial \eta} & 0 & \frac{\partial N^3}{\partial \eta} \\ \frac{\partial N^1}{\partial \eta} & \frac{\partial N^1}{\partial \xi} & \frac{\partial N^2}{\partial \eta} & \frac{\partial N^2}{\partial \xi} & \frac{\partial N^3}{\partial \eta} & 0 \end{bmatrix} \begin{bmatrix} u_\xi^1 \\ u_\eta^1 \\ u_\xi^2 \\ u_\eta^2 \\ u_\xi^3 \\ u_\eta^3 \end{bmatrix} \quad (25)$$

Note that although several of the displacements are zero (i.e. $u_\xi^1 = u_\eta^1 = u_\eta^2 = 0$) by virtue of the definition of the coordinate system, Eq. (25) is still useful because it can be used to compute the change in strain energy due to an arbitrary virtual displacement field to obtain the nodal

internal forces. For the linear triangular element it is possible to obtain a closed expression for the shape functions. However, a more general approach is to operate on a canonical element shape where the functions are especially simple and then use an isoparametric transform [11] to compute the shape function gradients. To this effect we use an additional transformed coordinate system (p-q) as shown in Figure 4.

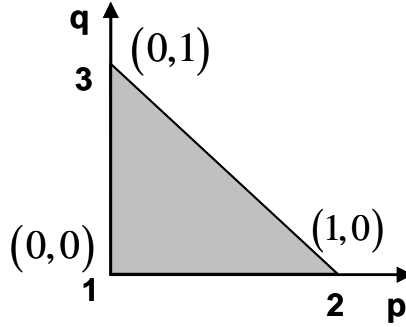


Figure 4. Transformed coordinate system and canonical element shape.

The shape functions then become

$$N^1 = 1 - p - q ; N^2 = p ; N^3 = q \quad (26)$$

and the transform from the p-q plane to the ξ - η system is given by the isoparametric transform

$$(\xi, \eta) = \sum_{j=2}^3 (\xi^j, \eta^j) N^j \quad (27)$$

Note that in Eq. (27) the sum does not include the first node because it is placed at the origin.

The gradients of the shape functions can be recovered from

$$\begin{bmatrix} \frac{\partial N^i}{\partial p} \\ \frac{\partial N^i}{\partial q} \end{bmatrix} = \begin{bmatrix} \frac{\partial \xi}{\partial p} & \frac{\partial \eta}{\partial p} \\ \frac{\partial \xi}{\partial q} & \frac{\partial \eta}{\partial q} \end{bmatrix} \begin{bmatrix} \frac{\partial N^i}{\partial \xi} \\ \frac{\partial N^i}{\partial \eta} \end{bmatrix} = \mathbf{J} \begin{bmatrix} \frac{\partial N^i}{\partial \xi} \\ \frac{\partial N^i}{\partial \eta} \end{bmatrix} \quad (28)$$

where \mathbf{J} is the Jacobian of the isoparametric transform. Its value can be obtained from Eq. (26) and (27) and is constant across the element (linear element)

$$\mathbf{J} = \begin{bmatrix} \xi^2 & 0 \\ \xi^3 & \eta^3 \end{bmatrix} \quad (29)$$

The inversion of the system (28) yields the gradients of the shape functions

$$\begin{bmatrix} \frac{\partial N^i}{\partial \xi} \\ \frac{\partial N^i}{\partial \eta} \end{bmatrix} = \mathbf{J}^{-1} \begin{bmatrix} \frac{\partial N^i}{\partial p} \\ \frac{\partial N^i}{\partial q} \end{bmatrix} \quad (30)$$

Once the strains (25) are known, the corresponding stresses are calculated assuming a plane stress state (an acceptable hypothesis for thin surface elements) and linear elastic isotropic behavior. Hence,

$$\begin{bmatrix} \sigma_\xi \\ \sigma_\eta \\ \tau_{\xi\eta} \end{bmatrix} = \frac{E}{1-\nu^2} \begin{bmatrix} \varepsilon_\xi + \nu\varepsilon_\eta \\ \varepsilon_\eta + \nu\varepsilon_\xi \\ \frac{1-\nu}{2}\gamma_{\xi\eta} \end{bmatrix} \quad (31)$$

As the membrane buckles under compressive loads, the stresses given by Eq. (31) must be corrected [15]. To this end, we shall refer to Eq. (31) as the trial stress state σ^t . Then, three possible membrane states, depicted in Figure 5, are considered:

- Taut: the minimum principal trial stress is positive. No corrections are needed.
- Wrinkled: membrane is not taut, but the maximum principal strain is positive. Trial state is replaced with a uniaxial stress state.
- Slack: the maximum principal strain is negative. The corrected stresses are zero.

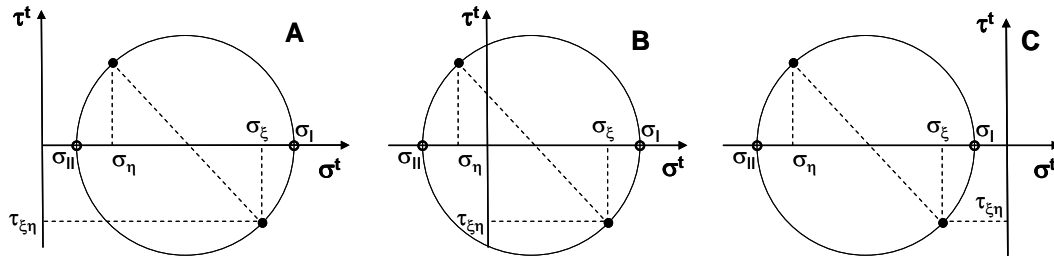


Figure 5. Trial membrane states: taut (A), wrinkled (B) and slack (C).

When the membrane is wrinkled the stress state is corrected (see Figure 6). First, the average in-plane direct strain, maximum shear strain and maximum principal strain are obtained from

$$\varepsilon_m = \frac{\varepsilon_\xi + \varepsilon_\eta}{2} ; \quad \frac{\gamma_{max}}{2} = \sqrt{\left(\frac{\varepsilon_\xi - \varepsilon_\eta}{2}\right)^2 + \frac{\gamma_{\xi\eta}^2}{4}} ; \quad \varepsilon_I = \varepsilon_m + \frac{\gamma_{max}}{2} \quad (32)$$

Using the values in expressions (32) the stress state is corrected in the principal strain directions and then rotated back to the ξ - η axes

$$\sigma_I = E\varepsilon_I ; \sigma_{II} = 0 ; \sigma_m = \frac{\sigma_I}{2} \quad (33)$$

$$\sigma_\xi = \sigma_m \left(1 + \frac{\varepsilon_\xi - \varepsilon_\eta}{\gamma_{\max}} \right) ; \sigma_\eta = \sigma_m \left(1 - \frac{\varepsilon_\xi - \varepsilon_\eta}{\gamma_{\max}} \right) ; \tau_{\xi\eta} = \sigma_m \frac{\gamma_{\xi\eta}}{\gamma_{\max}}$$

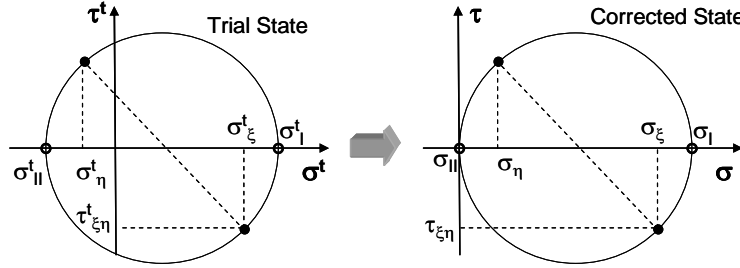


Figure 6. Stress correction for wrinkled membrane.

The elastic stresses are next augmented with viscous terms to include damping stresses. Using the nodal velocities, the components of the strain rate tensor can be computed. The damping stresses are then given by

$$\begin{bmatrix} \sigma_\xi \\ \sigma_\eta \\ \tau_{\xi\eta} \end{bmatrix}_{damp} = \frac{\beta E}{1-\nu^2} \begin{bmatrix} \dot{\varepsilon}_\xi + \nu \dot{\varepsilon}_\eta \\ \dot{\varepsilon}_\eta + \nu \dot{\varepsilon}_\xi \\ \frac{1-\nu}{2} \dot{\gamma}_{\xi\eta} \end{bmatrix} + b\rho c_d L (\dot{\varepsilon}_\xi + \dot{\varepsilon}_\eta) \begin{bmatrix} 1 \\ 1 \\ 0 \end{bmatrix} \quad (34)$$

The total (elastic and viscous) stress is used to calculate the nodal forces. This carried out by evaluating the change in strain energy due to a virtual displacement of the nodes. As the triangular linear elements create a constant strain (and stress) field at a single point, Gauss quadrature is adequate. This result

$$\int \boldsymbol{\sigma} : \delta \boldsymbol{\varepsilon} d\Omega = tA_0 (\sigma_\xi \delta \varepsilon_\xi + \sigma_\eta \delta \varepsilon_\eta + \tau_{\xi\eta} \delta \gamma_{\xi\eta}) \quad (35)$$

where t is the element thickness and A_0 its reference (undeformed) element area.

The external loads acting on the elements are introduced through the vector of generalized forces. For example, if the upper face of the element (the side towards which the normal vector \mathbf{n} points) is subject to a uniform pressure loading, the corresponding nodal generalized forces are written as

$$\begin{bmatrix} I_n^1 \\ I_n^2 \\ I_n^3 \end{bmatrix} = -\frac{pA_p}{3} \begin{bmatrix} 1 \\ 1 \\ 1 \end{bmatrix} \quad (36)$$

where A_p stands for current projected area of the element. Finally, once all the components of the internal forces have been determined on the local reference frame, the global force vector can be assembled. The transformation to the global inertial reference system is given by

$$\mathbf{I}_{\text{glob}}^i = I_{\xi}^i \mathbf{e}_1 + I_{\eta}^i \mathbf{e}_2 + I_n^i \mathbf{n} \quad (37)$$

3.1.4.3 Four-node linear tetrahedral solid element

In PARACHUTES, the solid elements are particularly intended to model suspended payloads. Hence, while only small strains are expected, the rigid body displacements involved can be very large and it is necessary to isolate the material behavior from these effects. To this end, similarly as with triangular elements, a corrotational formulation is adopted. The base of the tetrahedron is used to define the local corrotational reference frame.

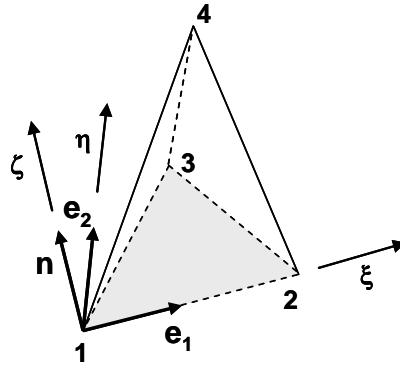


Figure 7. Tetrahedron corrotational reference frame.

The three unit vectors along the local axes are obtained from

$$\mathbf{e}_1 = \frac{\mathbf{x}^2 - \mathbf{x}^1}{\|\mathbf{x}^2 - \mathbf{x}^1\|} ; \quad \mathbf{n} = \frac{\mathbf{e}_1 \times (\mathbf{x}^3 - \mathbf{x}^1)}{\|\mathbf{e}_1 \times (\mathbf{x}^3 - \mathbf{x}^1)\|} ; \quad \mathbf{e}_2 = \mathbf{n} \times \mathbf{e}_1 \quad (38)$$

and any point \mathbf{x} of the tetrahedron can now be identified by its three local coordinates

$$(\xi, \eta, \zeta) = ((\mathbf{x} - \mathbf{x}^1) \cdot \mathbf{e}_1, (\mathbf{x} - \mathbf{x}^1) \cdot \mathbf{e}_2, (\mathbf{x} - \mathbf{x}^1) \cdot \mathbf{n}) \quad (39)$$

Due to this particular choice of coordinates, the vertices of the element no longer have completely arbitrary coordinates, as some of them are always null. We have,

$$\begin{aligned} \mathbf{x}^1 &= (0, 0, 0) & \mathbf{x}^2 &= (\xi^2, 0, 0) \\ \mathbf{x}^3 &= (\xi^3, \eta^3, 0) & \mathbf{x}^4 &= (\xi^4, \eta^4, \zeta^4) \end{aligned} \quad (40)$$

Therefore, it is possible to calculate the strain field inside the tetrahedron (which is constant for linear elements) as a function of only six variables. The interpolated displacement field is

$$(u_\xi, u_\eta, u_\zeta) = \sum_{j=2}^4 N^j (u_\xi^j, u_\eta^j) \quad (41)$$

where node 1 does not enter the sum as it remains always at the origin of the local frame. In order to calculate the gradients of the shape functions an isoparametric transformation is applied in order to perform the relevant operations on a simpler geometry. The transformed coordinate system is denoted as (p-q-r).

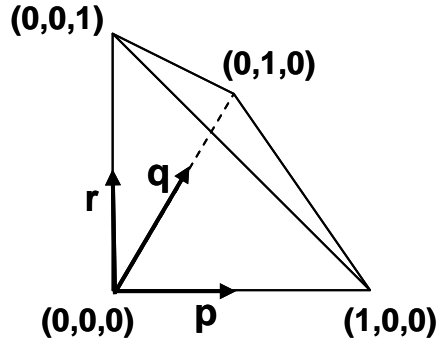


Figure 8. Tetrahedron reference coordinates in the p-q-r system.

The shape functions in the transformed system have very simple expressions:

$$N^1 = 1 - p - q - r ; N^2 = p ; N^3 = q ; N^4 = r \quad (42)$$

It can be observed in Eq. (42) that the four shape functions always add to one. The ξ - η - ζ coordinates of a point with known values of p-q-r are given by

$$(\xi, \eta, \zeta) = \sum_{j=2}^4 (\xi^j, \eta^j, \zeta^j) N^j \quad (43)$$

Using the chain rule the derivatives of the shape functions with respect to the transformed coordinates can be obtained from

$$\begin{bmatrix} \frac{\partial N^i}{\partial p} \\ \frac{\partial N^i}{\partial q} \\ \frac{\partial N^i}{\partial r} \end{bmatrix} = \begin{bmatrix} \frac{\partial \xi}{\partial p} & \frac{\partial \eta}{\partial p} & \frac{\partial \zeta}{\partial p} \\ \frac{\partial \xi}{\partial q} & \frac{\partial \eta}{\partial q} & \frac{\partial \zeta}{\partial q} \\ \frac{\partial \xi}{\partial r} & \frac{\partial \eta}{\partial r} & \frac{\partial \zeta}{\partial r} \end{bmatrix} \begin{bmatrix} \frac{\partial N^i}{\partial \xi} \\ \frac{\partial N^i}{\partial \eta} \\ \frac{\partial N^i}{\partial \zeta} \end{bmatrix} = \mathbf{J} \begin{bmatrix} \frac{\partial N^i}{\partial \xi} \\ \frac{\partial N^i}{\partial \eta} \\ \frac{\partial N^i}{\partial \zeta} \end{bmatrix} \quad (44)$$

The Jacobian of the isoparametric transform (\mathbf{J}) can be obtained from Eqs. (42) and (43), and is constant across the element

$$\mathbf{J} = \begin{bmatrix} \xi^2 & 0 & 0 \\ \xi^3 & \eta^3 & 0 \\ \xi^4 & \eta^4 & \zeta^4 \end{bmatrix} \quad (45)$$

The inversion of the system (44) yields the gradients sought

$$\begin{bmatrix} \frac{\partial N^i}{\partial \xi} \\ \frac{\partial N^i}{\partial \eta} \end{bmatrix} = \frac{1}{\xi_2 \eta_3 \zeta_4} \begin{bmatrix} -\eta_3 \zeta_4 & \eta_3 \zeta_4 & 0 & 0 \\ \xi_3 \zeta_4 - \xi_2 \zeta_4 & -\xi_3 \zeta_4 & \xi_2 \zeta_4 & 0 \\ \xi_4 \eta_3 - \xi_3 \eta_4 + \xi_2 \eta_4 - \xi_2 \eta_3 & \xi_3 \eta_4 - \xi_4 \eta_3 & -\xi_2 \eta_4 & \xi_2 \eta_3 \end{bmatrix} \quad (46)$$

The components of the strain tensor can now be determined easily from

$$\begin{bmatrix} \varepsilon_\xi \\ \varepsilon_\eta \\ \varepsilon_\zeta \\ \gamma_{\xi\eta} \\ \gamma_{\xi\zeta} \\ \gamma_{\eta\zeta} \end{bmatrix} = \begin{bmatrix} N_\xi^2 u_\xi^2 \\ N_\eta^3 u_\eta^3 \\ N_\zeta^4 u_\zeta^4 \\ N_\eta^2 u_\xi^2 + N_\eta^3 u_\xi^3 \\ N_\zeta^2 u_\xi^2 + N_\zeta^3 u_\xi^3 + N_\zeta^4 u_\xi^4 \\ N_\zeta^3 u_\eta^3 + N_\zeta^4 u_\eta^4 \end{bmatrix} \quad (47)$$

To keep the notation compact, a sub-index has been introduced in Eq. (47) to indicate derivation of the shape function with respect to a local coordinate ($N_{\eta}^k = \partial N^k / \partial \eta$). Similar to membrane elements, the null terms in Eq. (47) have been dropped to improve efficiency. The corresponding stresses are calculated assuming a linear elastic isotropic behavior. Hence,

$$\begin{aligned} \boldsymbol{\sigma} &= 2G\mathbf{e} + \sigma_h \mathbf{I} \\ \mathbf{e} &= \boldsymbol{\varepsilon} - \frac{\varepsilon_v}{3} \mathbf{I} ; \quad \varepsilon_v = \varepsilon_\xi + \varepsilon_\eta + \varepsilon_\zeta ; \quad \sigma_h = K \varepsilon_v \end{aligned} \quad (48)$$

The corresponding nodal generalized forces can be determined from the principle of virtual work. Given an arbitrary virtual displacement field, the work done by the nodal loads should equal the virtual change in strain energy

$$\sum_j \mathbf{F}^j \delta \mathbf{u}^j = \int_{\Omega_{el}} \boldsymbol{\sigma} : \delta \boldsymbol{\varepsilon} d\Omega \quad (49)$$

The virtual strain field is a linear combination of the gradients of the shape functions and the virtual nodal displacements given by

$$\begin{bmatrix} \delta \varepsilon_\xi \\ \delta \varepsilon_\eta \\ \delta \varepsilon_\zeta \\ \delta \gamma_{\xi\eta} \\ \delta \gamma_{\xi\zeta} \\ \delta \gamma_{\eta\zeta} \end{bmatrix} = \begin{bmatrix} N_\xi^1 \delta u_\xi^1 + N_\xi^2 \delta u_\xi^2 \\ N_\eta^1 \delta u_\eta^1 + N_\eta^2 \delta u_\eta^2 + N_\eta^3 \delta u_\eta^3 \\ N_\zeta^1 \delta u_\zeta^1 + N_\zeta^2 \delta u_\zeta^2 + N_\zeta^3 \delta u_\zeta^3 + N_\zeta^4 \delta u_\zeta^4 \\ N_\eta^1 \delta u_\xi^1 + N_\xi^1 \delta u_\eta^1 + N_\eta^2 \delta u_\xi^2 + N_\xi^2 \delta u_\eta^2 + N_\eta^3 \delta u_\xi^3 \\ N_\zeta^1 \delta u_\xi^1 + N_\xi^1 \delta u_\zeta^1 + N_\zeta^2 \delta u_\xi^2 + N_\xi^2 \delta u_\zeta^2 + N_\zeta^3 \delta u_\xi^3 + N_\xi^3 \delta u_\zeta^3 + N_\zeta^4 \delta u_\xi^4 \\ N_\zeta^1 \delta u_\eta^1 + N_\eta^1 \delta u_\zeta^1 + N_\zeta^2 \delta u_\eta^2 + N_\eta^2 \delta u_\zeta^2 + N_\zeta^3 \delta u_\eta^3 + N_\eta^3 \delta u_\zeta^3 + N_\zeta^4 \delta u_\eta^4 \end{bmatrix} \quad (50)$$

Notice that the expression for the virtual deformation field is far more complex than the formula for the strain field (47) (no single component of the virtual displacement field can be discarded beforehand). The internal force vector, obtained by combining Eqs. (49) and (50), results

$$\begin{bmatrix} I_\xi^1 \\ I_\eta^1 \\ I_\zeta^1 \\ I_\xi^2 \\ I_\eta^2 \\ I_\zeta^2 \\ I_\xi^3 \\ I_\eta^3 \\ I_\zeta^3 \\ I_\xi^4 \\ I_\eta^4 \\ I_\zeta^4 \end{bmatrix} = \Omega^{el} \begin{bmatrix} \sigma_\xi N_\xi^1 + \tau_{\xi\eta} N_\eta^1 + \tau_{\xi\zeta} N_\zeta^1 \\ \sigma_\eta N_\eta^1 + \tau_{\xi\eta} N_\xi^1 + \tau_{\eta\zeta} N_\zeta^1 \\ \sigma_\zeta N_\zeta^1 + \tau_{\xi\zeta} N_\xi^1 + \tau_{\eta\zeta} N_\eta^1 \\ \sigma_\xi N_\xi^2 + \tau_{\xi\eta} N_\eta^2 + \tau_{\xi\zeta} N_\zeta^2 \\ \sigma_\eta N_\eta^2 + \tau_{\xi\eta} N_\xi^2 + \tau_{\eta\zeta} N_\zeta^2 \\ \sigma_\zeta N_\zeta^2 + \tau_{\xi\zeta} N_\xi^2 + \tau_{\eta\zeta} N_\eta^2 \\ \tau_{\xi\eta} N_\eta^3 + \tau_{\xi\zeta} N_\zeta^3 \\ \sigma_\eta N_\eta^3 + \tau_{\eta\zeta} N_\zeta^3 \\ \sigma_\zeta N_\zeta^3 + \tau_{\eta\zeta} N_\eta^3 \\ \tau_{\xi\zeta} N_\zeta^4 \\ \tau_{\eta\zeta} N_\zeta^4 \\ \sigma_\zeta N_\zeta^4 \end{bmatrix} \quad (51)$$

where only the non-vanishing terms have been included for the sake of efficiency. The volume of the element is obtained from the isoparametric transform as

$$\Omega^{el} = \frac{|\mathbf{J}|}{6} = \frac{\xi_2 \eta_3 \zeta_4}{6} \quad (52)$$

In order to calculate the damping terms, the nodal velocities are transformed to the corrotational reference frame. This is a two-step process. First, the velocities of all the nodes are measured relative to the origin of the system (i.e. the first node). This yields the intermediate velocity \mathbf{w} whose components are given by:

$$(w_\xi^i, w_\eta^i, w_\zeta^i) = (\mathbf{v}_r^i \cdot \mathbf{e}_1, \mathbf{v}_r^i \cdot \mathbf{e}_2, \mathbf{v}_r^i \cdot \mathbf{n}) \quad \text{where} \quad \mathbf{v}_r^i = \mathbf{v}^i - \mathbf{v}^1 \quad (53)$$

Due to the choice of the reference frame, the following relationship must exist between the intermediate velocities and the angular velocity of the corrotational reference system

$$\begin{cases} w_\eta^2 = \Omega_\zeta \xi^2 \\ w_\zeta^2 = -\Omega_\eta \xi^2 \\ w_\zeta^3 = \Omega_\xi \eta^3 - \Omega_\eta \xi^3 \end{cases} \quad (54)$$

It is therefore easy to calculate the spin rate of the local reference frame

$$\mathbf{\Omega} : \left(\frac{w_\eta^2}{\xi^2}, -\frac{w_\zeta^2}{\xi^2}, \frac{1}{\eta^3} \left(w_\zeta^3 - \frac{w_\zeta^2}{\xi^2} \xi^3 \right) \right) \quad (55)$$

Subtracting the spin-induced components from the intermediate velocities, the corrotational velocities are finally obtained

$$\begin{aligned} \tilde{\mathbf{v}}^1 &: (0, 0, 0) \\ \tilde{\mathbf{v}}^2 &: (w_\xi^2, 0, 0) \\ \tilde{\mathbf{v}}^3 &: (w_\xi^3 + \Omega_\zeta \eta^3, w_\eta^3 - \Omega_\zeta \xi^3, 0) \\ \tilde{\mathbf{v}}^4 &: (w_\xi^4 - \Omega_\eta \zeta^4 + \Omega_\zeta \eta^4, w_\eta^4 + \Omega_\xi \zeta^4 - \Omega_\zeta \xi^4, w_\zeta^4 - \Omega_\xi \eta^4 + \Omega_\eta \xi^4) \end{aligned} \quad (56)$$

In Eq. (56) the tilde denotes a value measured in the corrotational frame of reference. The latter equation can be used with Eq. (47) to obtain the components of the strain rate tensor

$$\begin{bmatrix} \dot{\epsilon}_\xi \\ \dot{\epsilon}_\eta \\ \dot{\epsilon}_\zeta \\ \dot{\gamma}_{\xi\eta} \\ \dot{\gamma}_{\xi\zeta} \\ \dot{\gamma}_{\eta\zeta} \end{bmatrix} = \begin{bmatrix} N_\xi^2 \tilde{v}_\xi^2 \\ N_\eta^3 \tilde{v}_\eta^3 \\ N_\zeta^4 \tilde{v}_\zeta^4 \\ N_\eta^2 \tilde{v}_\xi^2 + N_\eta^3 \tilde{v}_\zeta^3 \\ N_\zeta^2 \tilde{v}_\xi^2 + N_\zeta^3 \tilde{v}_\eta^3 + N_\zeta^4 \tilde{v}_\xi^4 \\ N_\zeta^3 \tilde{v}_\eta^3 + N_\zeta^4 \tilde{v}_\eta^4 \end{bmatrix} \quad (57)$$

In order to improve performance the elastic stresses and the stiffness proportional terms from the Rayleigh damping are computed together in a single step. To this effect an equivalent strain tensor is defined as

$$\boldsymbol{\epsilon}^{\text{eq}} = \boldsymbol{\epsilon} + \beta \dot{\boldsymbol{\epsilon}} \quad (58)$$

The equivalent strain is used in the constitutive law (48) to include the damping term in an efficient way. Additionally, a linear bulk viscosity is included to reduce high frequency ringing. Thus, an additional hydrostatic stress is included in the material computations

$$\sigma_h^{\text{bv}} = b_1 \rho c_d L_e \dot{\epsilon}_{\text{vol}} \quad (59)$$

The fraction of the critical damping (needed to calculate the stability limit) due to the effect of the bulk viscous stress is

$$\xi^{bv} = b_1 \quad (60)$$

Once all nodal loads have been calculated on the corrotational frame, the contribution to the global force vector (which is always expressed in global coordinates) is obtained from

$$\mathbf{I}_{\text{glob}}^i = I_{\xi}^i \mathbf{e}_1 + I_{\eta}^i \mathbf{e}_2 + I_{\zeta}^i \mathbf{n} \quad (61)$$

The mass matrix for the element, assuming uniform density, is

$$\mathbf{M} = \frac{\rho \Omega^{el}}{20} \begin{bmatrix} 2 & 1 & 1 & 1 \\ 1 & 2 & 1 & 1 \\ 1 & 1 & 2 & 1 \\ 1 & 1 & 1 & 2 \end{bmatrix} \quad (62)$$

Therefore, the lumped mass becomes

$$\mathbf{M}^d = \frac{\rho \Omega^{el}}{4} \begin{bmatrix} 1 & 0 & 0 & 0 \\ 0 & 1 & 0 & 0 \\ 0 & 0 & 1 & 0 \\ 0 & 0 & 0 & 1 \end{bmatrix} \quad (63)$$

A safe estimate of the allowable time step is given by the minimum height of the element

$$L_e = \frac{3\Omega^{el}}{\max(A^i)} \quad (64)$$

3.1.5 Additional features

In order to complete the description of the structural module developed for PARACHUTES, other important characteristics of the solver regarding the modelling of payloads and cables are described in this section.

3.1.5.1 Rigid body modelling

The deformation of the payload and other suspended bodies is usually negligible if compared to the rest of the structure. Therefore, these can be considered as rigid bodies without affecting the behavior of the system, and large computational savings can be obtained. A rigid body has only 6 degrees of freedom and it has no upper bound on its allowable time step, therefore it can be included in the model at virtually no extra cost. PARACHUTES allows for arbitrary element sets of the model (of cable, membrane or solid type) to be converted into a rigid body, whose motion is fully characterized by its orientation and the position of its center of mass. The motion of the latter is solved by Eqs. (6) and (7), and the resultant attitude of the rigid body is obtained from

$$\mathbf{I}^G \cdot \frac{d\boldsymbol{\Omega}}{dt} = \mathbf{M}^G - \boldsymbol{\Omega} \otimes (\boldsymbol{\Omega} \cdot \mathbf{I}^G) \quad (65)$$

where \mathbf{I}^G denotes the tensor of inertia of the solid with respect to its center of mass, $\boldsymbol{\Omega}$ is the angular velocity and \mathbf{M}^G is the torque acting on the solid (due to both, external loads and internal forces exerted by surrounding deformable elements). Eq. (65) is evaluated in a corotational frame which coincides with the principal axes of inertia of the rigid body. Thus, the angular acceleration can be computed without matrix inversion because the moment of inertia tensor is diagonal. The inertial properties of the elements making up the rigid body are automatically computed during preprocessing and the elements are removed from the analysis. The trajectories of the nodes belonging to the rigid body are calculated at the end of each step in terms of the translation of the center of mass and the total rotation of the body.

It is important to note that PARACHUTES allows accounting for aerodynamic forces acting on rigid suspended bodies also by means of prescribed aerodynamic functions, obtained for example from experimental data fitting in terms of the body shape and attitude. The current version of the program allows only to prescribe drag functions defined in terms of the body projected area (details are given in the Program User's Manual [16]). Experimental data useful for typical cargo containers can be found in [17, 18].

3.1.5.2 Internal computation of the cable drag forces

The wind loads acting on the suspension and control lines are treated in PARACHUTES in a simplified manner. The chords are considered as long circular cylinders exposed to the wind, and proper experimental drag coefficients are specified to calculate the aerodynamic load. This computation is carried out into the structural solver and the resultant forces are added to the element nodal force vector. At each node of the cable elements exposed to the wind, the aerodynamic drag load (per unit length) is computed by

$$\mathbf{f}^i = \frac{1}{2} \rho_\infty D C_D |\mathbf{v}_t^i| \mathbf{v}_t^i \quad (66)$$

where ρ_∞ , D and C_D denote the air density, cable diameter and cylinder drag coefficient (based on the diameter). The transverse wind velocity \mathbf{v}_t^i is given by

$$\mathbf{v}_t^i = -\mathbf{v}^i + (\mathbf{v}^i \cdot \mathbf{e}_1) \mathbf{e}_1 \quad (67)$$

being \mathbf{v}^i the node velocity and \mathbf{e}_1 a unit vector tangent to the cable. The procedure proposed yields the natural amount of damping required to obtain a realistic behavior of the suspension lines. This is achieved without the user having to tune any damping parameter and thus improves simultaneously the accuracy of the solution and the user friendliness of the software.

3.1.5.3 Control over changes in cable length

In order to simulate maneuvers or to achieve a desired flight configuration, a change in the length of the parachute control lines is typically required. As described in Section 3.1.4.1, this is done in PARACHUTES by introducing prescribed cable deformations through a change of the undeformed cable length. To simplify the simulation of maneuvers while improving the results, the prescribed cable deformations are entered in a tabular form, and the solver automatically interpolates the input values to ensure that the first and second time derivatives of the prescribed strains are continuous functions. A fifth-order piecewise polynomial (quintic splines) interpolation is used. This ensures that the accelerations created at the ends of the control lines change smoothly over time and do not excite high frequency modes of the system. Refer to the Program User's Manual for further details.

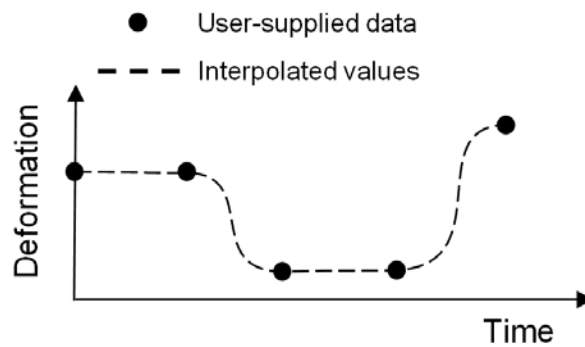


Figure 9. Smoothing of prescribed strain history.

3.2 The aerodynamic model

Under the assumption that a potential flow approximation is valid for nominal flight conditions of ram-air (gliding) parachutes, an unsteady low-order panel method is adopted in PARACHUTES. The aerodynamic problem to be solved consists of an arbitrary body (the parachute-payload system) immersed in an ideal fluid filling a domain Ω with far-field boundary S_∞ . The body contour is defined by S_B , and S_W represents the upper (U) and lower (L) sides of a thin wake extending downstream from the body. The boundaries S_B+S_W divide the problem domain into external and internal regions having harmonic potentials Φ and Φ_i , respectively (see Figure 10).

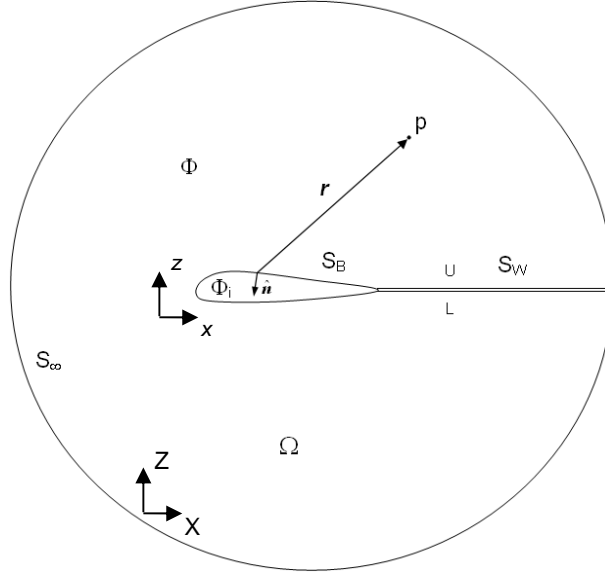


Figure 10. Aerodynamic problem setup.

To simplify the treatment of unsteady problems, a body-fixed coordinate system (x,y,z) and an inertial reference frame (X,Y,Z) are defined. The body system is attached to the body and follows its motion during the simulation. At time $t = t_0$ both coordinates systems are coincident with no relative motion; at time $t > t_0$, the position and orientation of the body system are determined either by the calculated body displacement or prescribed by flight path data.

In order to solve the problem described above, a general solution for the velocity potential Φ at any point p can be obtained by applying Green's theorem [19]. This yields

$$\Phi_p = \frac{1}{4\pi} \iint_{S_B} \mu \nabla \left(\frac{1}{r} \right) \cdot \hat{n} dS - \frac{1}{4\pi} \iint_{S_B} \left(\frac{\sigma}{r} \right) dS + \frac{1}{4\pi} \iint_{S_W} \mu_w \nabla \left(\frac{1}{r} \right) \cdot \hat{n} dS + \phi_\infty(p) \quad (68)$$

where r is the distance between the point p and a surface element dS having normal vector \hat{n} pointing outside Ω , ϕ_∞ is a constant freestream potential due to S_∞ and no jump in the normal component of the velocity across the wake is considered (thin wake assumption). The terms $-\mu = \Phi - \Phi_i$ and $-\sigma = \nabla(\Phi - \Phi_i) \cdot \hat{n}$ represent the strength (per unit area) of doublet and source surface distributions. These functions account for jumps in the potential and the normal component of the velocity across the boundaries, respectively.

In order to solve Eq. (68), the internal Dirichlet condition $\Phi_i = \text{const.} = \phi_\infty$ is applied. The velocity potential can be split into a freestream potential ϕ_∞ plus a perturbation potential due to the body and its wake given by $\phi = \Phi - \phi_\infty$. For a point p inside the body Eq. (68) becomes

$$0 = \frac{1}{4\pi} \iint_{S_B} \mu \nabla \left(\frac{1}{r} \right) \cdot \hat{n} dS - \frac{1}{4\pi} \iint_{S_B} \left(\frac{\sigma}{r} \right) dS + \frac{1}{4\pi} \iint_{S_W} \mu_w \nabla \left(\frac{1}{r} \right) \cdot \hat{n} dS \quad (69)$$

where the doublet strength turns into the perturbation velocity potential $-\mu = \phi = \Phi - \phi_\infty$ and the source strength is $-\sigma = \nabla(\Phi - \phi_\infty)$.

At this point some assumptions must be done to solve for Eq. (69). Regarding the source distribution, it is considered that the normal velocity across the body boundaries is zero (slip condition) or a known value (transpiration velocity). Hence, the source strengths σ can be determined through Neumann boundary conditions [19] by

$$\sigma = -\mathbf{V}_T - \mathbf{v} \cdot \hat{\mathbf{n}} = -\mathbf{V}_T - (\mathbf{V}_0 + \boldsymbol{\omega} \times \mathbf{r} + \mathbf{v}_{rel}) \cdot \hat{\mathbf{n}} \quad (70)$$

In Eq. (70) \mathbf{v} is the instantaneous kinematic velocity. It depends on the velocity of the body system's origin \mathbf{V}_0 , the spin rate $\boldsymbol{\omega}$ of the body (as a rigid solid) and relative velocities \mathbf{v}_{rel} caused by deformations in the body's frame. \mathbf{V}_T is a specified normal velocity, relative to the boundary (transpiration velocity), which is null if the latter are airtight. The second assumption adopted concerns the wake behavior. Here, the Kutta condition [19] is used to determine the wake doublet strength μ_w in terms of the body doublets. This empirical-based condition, which enforces zero resultant vorticity along shedding lines, allows the flow to separate smoothly at body trailing edges and fixes the correct amount of circulation for lifting problems. Once the source and wake doublet distributions have been determined, it is possible to solve Eqs. (69) for the unknown doublet distribution along body μ .

In aerodynamic analyses is often needed to consider certain components that are extremely thin. Particularly in the present context, where there are fabrics in the parachute that are exposed to the wind, but not always form a closed body. In such cases, the upper and lower sides of the thin body are collapsed into a sheet across the same the normal component of the velocity is assumed to be continuous. Then, an equation for thin boundaries can be obtained through the so-called Neumann condition. At a given point p , this is achieved by replacing the perturbation velocity (obtained by differentiating Eq.(68)) into the slip boundary condition ($(\nabla\Phi - \mathbf{v}) \cdot \mathbf{n} = 0$). This procedure gives

$$\frac{1}{4\pi} \iint_{S_B} \mu \hat{\mathbf{n}}_p \cdot \nabla \left(\hat{\mathbf{n}} \cdot \nabla \left(\frac{1}{r} \right) \right) dS + \frac{1}{4\pi} \iint_{S_w} \mu_w \hat{\mathbf{n}}_p \cdot \nabla \left(\hat{\mathbf{n}} \cdot \nabla \left(\frac{1}{r} \right) \right) dS - \hat{\mathbf{n}}_p \cdot \mathbf{v} = 0 \quad (71)$$

which is solved for the doublet distribution on thin aerodynamic surfaces. Note that the source contributions are zero in Eq. (71) as the normal component of the velocity is assumed to be constant across thin boundaries. However, if aerodynamic configurations having mixed thin/thick surfaces are considered, the contribution to the normal component of the velocity due to the source distribution on thick boundaries must be accounted for in Eq. (71).

In order to solve Eqs. (69) and (71) for arbitrary configurations, the latter must be discretized by breaking down the surface integrals into integrals over quadrilateral and/or triangular flat panels distributed along the body and the wake. The resultant system of equations is solved algebraically, and iterative and direct solvers are available in PARACHUTES for this purpose (see the Program User's Manual [16]). Note that the kinematic velocity changes in time as a consequence of the body motion. This introduces time dependence in the potential problem. The solution procedure followed in PARACHUTES is described below.

3.2.1 Numerical solution of the potential flow problem

The discrete forms of Eqs. (69) and (71) are obtained by discretizing the body boundaries S_B into N_B triangular or quadrilateral flat surface panels forming a surface grid. The wake surface S_W is assumed to be composed of N_W quadrilateral panels developing from specified shedding lines on the body. Each panel is identified by its vertices, a particular point named *control point* and a local system of coordinates. The control point is located at the centroid of the panel, on the surface or slightly inside the body. The panel coordinate system, whose origin is located at the control point, is defined by a unit outward normal vector \hat{n} and a set of unit tangent vectors \hat{l} and \hat{m} . Figure 11 shows a typical panel discretization of a parachute canopy and its wake.

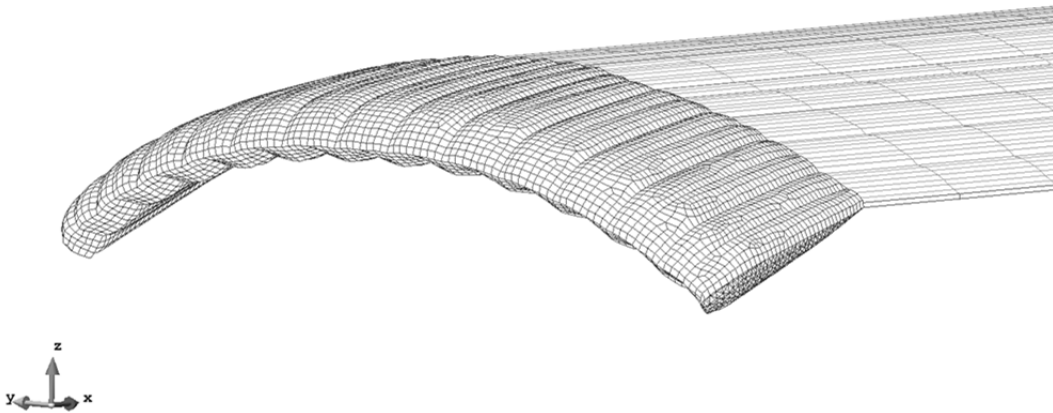


Figure 11. Typical canopy and wake discretization.

The discretized form of the integral governing equations is obtained by breaking down the surface integrals over S_B and S_W into integrals over the panels. Since the doublet and source strengths are constant on each panel (low-order method), these terms can be factored out of the integrals, allowing the latter to be solved in a closed manner. Then, the discrete equations are satisfied at each control point $J = 1, N_B$ on the body by considering the contribution of all the panels $K = 1, N_B + N_W$. According to this procedure, the discrete internal Dirichlet condition (Eq. (69)) is written for each control point $J = 1, N_B^{thick}$ on thick boundaries by

$$\sum_{K=1}^{N_B} \mu_K C_{JK} + \sum_{L=1}^{N_W} \mu_L C_{JL} = \sum_{K=1}^{N_B} \sigma_K B_{JK} \quad (72)$$

where C_{JK} and B_{JK} denote, respectively, the perturbation potentials (per unit strength) at a control point J caused by the doublet and source constant distributions of a panel K . These perturbation potentials (also named influence coefficients) are given by

$$C_{JK} = \iint_{S_K} \nabla_K \left(\frac{1}{r_{JK}} \right) \hat{\mathbf{n}}_K dS_K \quad (73)$$

$$B_{JK} = \iint_{S_K} \frac{1}{r_{JK}} dS_K \quad (74)$$

being $\hat{\mathbf{n}}_K$ and dS_K the normal vector and a differential surface area of panel K , respectively. The distance r_{JK} is measured from the control point K to the control point J , i.e. $r_{JK} = \|\mathbf{x}_J - \mathbf{x}_K\|$, and the gradient is computed with respect to the coordinates of panel K . It should be pointed out that the surface integrals become singular when $r_{JK} \rightarrow 0$. For that special case, a slightly different approach is followed when deriving Eq. (68), see for instance [19]. This leads to $\Phi_p = -(\Phi - \Phi_i)/2 = \mu/2$ when p is inside the body. Accordingly, $C_{JJ} = 2\pi$ is enforced in Eq. (73) when evaluating the panel influence on itself.

Similarly, Eq. (71) is discretized for each control point $J = 1, N_B^{thin}$ on thin surfaces as

$$\sum_{K=1}^{N_B} \mu_K E_{JK} + \sum_{L=1}^{N_W} \mu_L E_{JL} = \sum_{K=1}^{N_B} \sigma_K D_{JK} + \hat{\mathbf{n}}_J \cdot \mathbf{v} + V_{N_J} \quad (75)$$

where \mathbf{v} is the instantaneous kinematic velocity given by Eq. (70), V_{N_J} denotes a prescribed normal velocity relative to the boundary and $\hat{\mathbf{n}}_J$ is the unit normal vector at the control point J . The normal components of the perturbation velocity at a control point J due to constant doublet and source distributions (per unit strength) on panel K are obtained by

$$E_{JK} = \hat{\mathbf{n}}_J \cdot \mathbf{V}_{\mu_{JK}} \quad (76)$$

$$D_{JK} = \hat{\mathbf{n}}_J \cdot \mathbf{V}_{\sigma_{JK}} \quad (77)$$

with

$$\mathbf{V}_{\mu_{JK}} = \frac{1}{4\pi} \iint_{S_K} \nabla_J \left(\hat{\mathbf{n}}_K \cdot \nabla_K \left(\frac{1}{r_{JK}} \right) \right) dS_K \quad (78)$$

$$\mathbf{V}_{\sigma_{JK}} = \frac{1}{4\pi} \iint_{S_K} \nabla_J \left(\frac{1}{r_{JK}} \right) dS_K \quad (79)$$

In spite of the fact that the source distribution vanishes for thin surface panels (there is no jump in the normal velocity, see Eq. (71)), the influence coefficient D_{JK} is included in the

discrete Eq. (75) to account for the perturbation velocity induced on thin panels by source distributions placed on thick panels (for configurations presenting mixed thin/thick boundaries).

3.2.1.1 Calculation of the influence coefficients

The influence coefficients, given by Eqs. (73) and (74) for the velocity potential and Eqs. (78) and (79) for the velocity vector, are computed in a closed manner following the procedure presented in [6]. Accordingly, the integrals on a given panel are evaluated by adding individual contributions of its edges (rounded in a counter-clockwise sense). This fact allows quadrilateral and triangular panels (as a matter of fact any closed polygonal panel) to be treated in a similar manner.

The geometrical model employed for the calculations is presented in Figure 12. Each panel is geometrically defined by the position of its vertices $\mathbf{R}_1, \mathbf{R}_2, \dots, \mathbf{R}_n$ (numbered in a counter-clockwise sense according to the panel's outward normal vector), the control point given by $\mathbf{R}_C = (\sum_{i=1}^n \mathbf{R}_i)/n$ and a set of unit normal and tangent vectors. The normal vector \mathbf{n} is computed by the cross product of the panel's diagonals. The first tangent vector \mathbf{m} is generated between the control point and the mid-point of one of the panel sides, e.g $\mathbf{m} = (\mathbf{R}_3 + \mathbf{R}_4)/2 - \mathbf{R}_C$ in a quadrilateral, and the second tangent vector \mathbf{l} is defined to be orthogonal to \mathbf{m} and \mathbf{n} , i.e $\mathbf{l} = \mathbf{m} \times \mathbf{n}$. Then, these vectors are normalized ($\hat{}$).

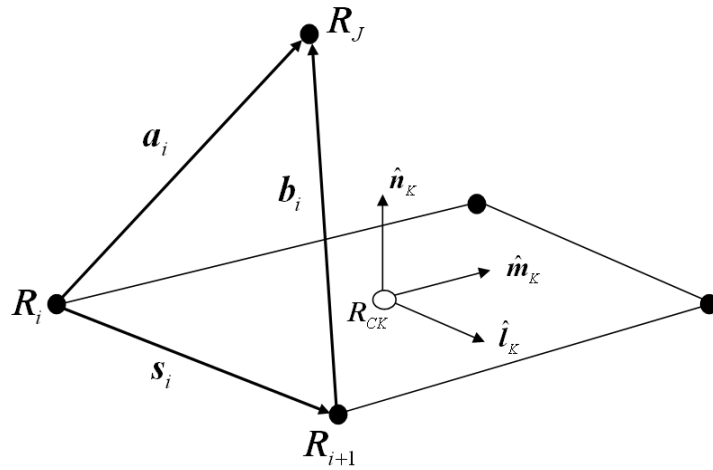


Figure 12. Geometrical arrangement for the evaluation of the panel influence coefficients.

The influence of a panel K on a point J is computed exclusively by the geometry of the panel K and the coordinates of the point J where the panel's influence is sought. Previous to the calculations, the panel vertices \mathbf{R}_i and the point \mathbf{R}_J are converted to the panel local system, defined by the unit vectors $(\hat{\mathbf{l}}_K, \hat{\mathbf{m}}_K, \hat{\mathbf{n}}_K)$ with origin at the control point \mathbf{R}_{CK} . Then, each panel side is defined as $\mathbf{s}_i = \mathbf{R}_{i+1} - \mathbf{R}_i$ and three auxiliary vectors are introduced: $\mathbf{a}_i = \mathbf{R}_J - \mathbf{R}_i$, $\mathbf{b}_i =$

$\mathbf{R}_j - \mathbf{R}_{i+1}$ and $\mathbf{P}_{JK} = \mathbf{R}_j - \mathbf{R}_{CK} = \mathbf{R}_j$ (in panel coordinates). Note that $\mathbf{a}_i = \mathbf{b}_{i-1}$ when the panel is rounded in a counter-clockwise sense.

Following the former definitions, the influence coefficients for constant strength doublet and source panels are computed. These coefficients are presented in the next sections (derivation details can be found in [6]).

3.2.1.2 Velocity potential influence coefficients

The velocity potential at a given point J due to a unit doublet constant distribution on panel K is given by Eq. (73). This integral can be computed as

$$C_{JK} = \sum_{i=1,n} C_{JK_i} \quad (80)$$

where C_{JK} is the contribution of each panel side s_i . Following the VSAERO [6] nomenclature,

$$C_{JK_i} = \tan^{-1} \left(\frac{RNUM}{DNOM} \right) \quad (81)$$

with

$$\begin{aligned} RNUM &= SM * PN * (B * PA - A * PB) \\ DNOM &= PA * PB + PN^2 * A * B * SM^2 \end{aligned} \quad (82)$$

where

$$\begin{aligned} PN &= \mathbf{P}_{JK} \cdot \hat{\mathbf{n}}_K \quad (= P_{JK} \text{ (3)}) \\ A &= \|\mathbf{a}_i\| \\ B &= \|\mathbf{b}_i\| \\ PA &= PN^2 * SL + A1 * AM \quad (= \mathbf{a}_i \cdot [\hat{\mathbf{l}}_K \times (\mathbf{a}_i \times \mathbf{s}_i)]) \\ PB &= PN^2 * SL + A1 * BM = PA - A1 * SM \\ A1 &= AM * SL - AL * SM \quad (= \hat{\mathbf{n}}_K \cdot (\mathbf{s}_i \times \mathbf{a}_i)) \\ SL &= \mathbf{s}_i \cdot \hat{\mathbf{l}}_K \quad (= s_1) \\ AL &= \mathbf{a}_i \cdot \hat{\mathbf{l}}_K \quad (= a_1) \\ SM &= \mathbf{s}_i \cdot \hat{\mathbf{m}}_K \quad (= s_2) \\ AM &= \mathbf{a}_i \cdot \hat{\mathbf{m}}_K \quad (= a_2) \\ BM &= \mathbf{b}_i \cdot \hat{\mathbf{m}}_K \quad (= b_2) \end{aligned} \quad (83)$$

Following a similar approach, the velocity potential at a given point J due to a unit constant strength on panel K (Eq. (74)) is computed by

$$B_{JK} = \sum_{i=1,n} B_{JK_i} \quad (84)$$

The contribution of each panel side s_i is

$$B_{JK_i} = A1 * GL - PN * C_{JK_i} \quad (85)$$

where the coefficients $A1$ and PN are given in Eqs. (83), C_{JK_i} is the side contribution of the doublet (Eq. (81)) and the GL term is

$$GL = \frac{1}{s} \log \left| \frac{A + B + s}{A + B - s} \right| \quad (86)$$

being $s = \|\mathbf{s}_i\|$ the side length.

If the control point J is far from the panel K , the computational cost of evaluating the influence coefficients can be reduced using far-field approximations. In such a case, the distributed singularity on the panel K is treated as a point singularity. The influence coefficients are [6]

$$C_{JK} = \frac{PN * A_K}{P_{JK}^3}, \quad B_{JK} = \frac{A_K}{P_{JK}} \quad (87)$$

where $P_{JK} = \|\mathbf{P}_{JK}\|$ is the distance between the points K and J , A_K denotes the surface area of panel K , and PN is given in Eqs. (83). The far-field approximations (87) are much simpler to evaluate and allow significant cost savings without affecting the solution accuracy. In PARACHUTES the far-field approximation is used when $P_{JK} > c_1 h_K$, being c_1 a constant (typically 5) and h_K a characteristic panel length. The latter is calculated as the maximum of the distances between the control point and the sides' mid-point.

3.2.1.3 Velocity vector influence coefficients

The velocity induced at a given point J due to a unit doublet distribution on panel K is given by Eq. (78). Similarly to the velocity potential, this integral can be calculated by [6]

$$\mathbf{V}_{\mu_{JK}} = \frac{1}{4\pi} \sum_{i=1,n} \mathbf{V}_{\mu_{JK_i}} \quad (88)$$

being the contribution of each panel side

$$\mathbf{V}_{\mu_{JK_i}} = \frac{\mathbf{a}_i \times \mathbf{b}_i * (A + B)}{A * B * (A * B + \mathbf{a}_i \cdot \mathbf{b}_i)} \quad (89)$$

where all the variables involved have been defined in Eqs. (83). Note that a finite-core model can be applied to avoid singularities in Eq. (89) when it is evaluated on panel's sides [6, 19].

The velocity induced at point J by a unit constant source distribution on panel K results

$$\mathbf{V}_{\sigma_{JK}} = \frac{1}{4\pi} \sum_{i=1,n} \mathbf{V}_{\sigma_{JK_i}} \quad (90)$$

being the side contribution

$$\mathbf{V}_{\sigma_{JK_i}} = GL * (SM * \hat{\mathbf{l}}_K - SL * \hat{\mathbf{m}}_K) + C_{JK_i} * \hat{\mathbf{n}}_K \quad (91)$$

where GL is given by Eq. (86), C_{JK_i} by Eq. (81) and the rest of variables are defined in Eqs. (83). Similarly to the perturbation potentials, if the point of interest J is located far from panel K the induced velocities can be approximated by far-field formulae. This gives

$$\begin{aligned} \mathbf{V}_{\mu_{JK}} &= \frac{A_K}{P_{JK}^5} * (3 * PN * \mathbf{P}_{JK} - P_{JK}^2 * \hat{\mathbf{n}}_K) \\ \mathbf{V}_{\sigma_{JK}} &= \frac{A_K}{P_{JK}^3} * \mathbf{P}_{JK} \end{aligned} \quad (92)$$

being A_K the surface area of panel K .

3.2.2 Wake treatment

The wake extending from the body is modelled in PARACHUTES by means of a time-steeping technique [5]. In this way, the wake develops according to the motion of the body during a time-marching simulation. The wake doublecity of the panels shed into the wake is determined by enforcing the Kutta condition at the shedding lines (no additional unknowns are introduced in the system). Due to the conservation of vorticity, the doublecity of the fluid particles forming the wake must not change and the wake strength is convected downstream. In addition, at the end of each time step a wake rollup procedure [19] is performed to align the wake panels with the local flow streamlines.

3.2.3 Computation of aerodynamic loads

The aerodynamic loads acting on the body are computed by means of the unsteady Bernoulli's equation. Thus, the coefficient of pressure (C_p) can be calculated at any point as

$$C_p = \frac{p - p_\infty}{\frac{1}{2} \rho_\infty V_\infty^2} = 1 - \left(\frac{V}{V_\infty} \right)^2 - \frac{2}{V_\infty^2} \frac{\partial \phi}{\partial t} \quad (93)$$

being V the magnitude of the total velocity at the control point (kinematic+perturbation) and V_∞ the magnitude of the reference freestream velocity. The unsteady term in Eq. (93) can be approximated by $\partial \phi / \partial t = -\partial \mu / \partial t = -(\mu_i - \mu_{t-\Delta t}) / \Delta t$. The tangential components of the perturbation velocity are evaluated by taking the gradient of μ in panel coordinates. Hence,

$$q_l = \frac{\partial \mu}{\partial \hat{\mathbf{l}}} \quad , \quad q_m = \frac{\partial \mu}{\partial \hat{\mathbf{m}}} \quad (94)$$

and the normal component of the velocity is given by

$$q_n = \sigma \quad (95)$$

being σ the panel's source strength (Eq. (70)). The total velocity on a given panel is obtained by adding the perturbation velocity to the instantaneous local kinematic velocity, i.e.

$$\mathbf{V} = q_l \hat{\mathbf{l}} + q_m \hat{\mathbf{m}} + q_n \hat{\mathbf{n}} + (\mathbf{V}_0 + \boldsymbol{\omega} \times \mathbf{r} + \mathbf{v}_{rel}) \quad (96)$$

Despite the fact that the evaluation of Eqs. (94) can be easily performed on structured discretizations (e.g. by using finite differences), a more general approach is needed for arbitrary body discretizations. In PARACHUTES the derivatives are evaluated in each panel using linear FE approximations. To this end, the values of the doublet strength at the panel vertices are obtained by nodal weighted averaging. At each vertex i we state,

$$\mu^i = \frac{\sum_{J=1,ns_i} A_J \mu_J}{\sum_{J=1,ns_i} A_J} \quad (97)$$

where A_J and μ_J are the surface area and doublet strength of a panel J , respectively, and the summation is performed over the ns_i panels surrounding the vertex. As mentioned before, once the doublet strengths at the panel's corner points are determined, the derivatives (94) are evaluated (in panel coordinates) by using a linear FE approximation.

3.2.4 Treatment of the canopy internal flow

The flow inside the parachute cells is not resolved by PARACHUTES, and only a constant pressure is applied inside the canopy to keep it pressurized. Stagnation pressure or a slightly lower value can be used if there is not a better estimate available (see comments below).

It is important to note that from the point of view of the aerodynamic model, the canopy inlet must be panelized to obtain the closed body shape required. Thus, the internal pressure applied does not generate a net resultant force. From the point of view of the structural model the requirements are different, and something must be done to prevent the inlet panels interfere with the structural behavior of the canopy (recall that both models share the same mesh). The procedure adopted in PARACHUTES is to enforce no aerodynamic load on the inlet panels and assign them very small relative thickness and Young's modulus. In this way, the inlet load bearing capacity and mass are negligible if compared with the rest of canopy panels and this approximates an open inlet.

Using the procedure above, from the structural point of view the canopy is no longer a closed body (pressure is zero on the inlet panels) and, thus, the internal pressure generates a net

resultant force. This contribution will be mainly aligned in the longitudinal direction, especially affecting the canopy drag. This is desired because also occurs in the real problem, but the internal pressure must be adjusted according to actual values for a more accurate modelling of the problem. Note that simply using stagnation pressure overestimates this force contribution because in the real model the airflow within the cells and the fabric porosity prevent from achieving stagnant pressures.

3.2.5 Robustness control

The proposed methodology for solving the aerodynamic problem in PARACHUTES is highly efficient; however, the particular characteristics of the problem to be solved may bring about some robustness issues. For instance, the parachute deformation and fabric wrinkling can cause excessive distortion of the aerodynamic grid, and intersection of panels can also occur in areas where the wake crosses the parachute canopy (or other aerodynamic bodies). Both distorted and intersected panels can cause very large entries in the aerodynamic influences matrix (Eqs. (69) and (71)), increasing its condition number and making difficult to solve it with accuracy (sometimes causing instability of the solution procedure). Distorted or wrinkled aerodynamic panels can also present problems when computing the aerodynamic loads, due to errors in the computation of spatial derivatives over these surface panels (see Eqs. (94)). Therefore, some degree of control is required over all these situations, which unfortunately are likely to occur during the simulations.

In order to counteract these problems, on the one hand, different types of controls are implemented to avoid large entries in the global coefficients matrix. These are based on panel's proximity criteria (when computing influences) and a control of the magnitudes involved. On the other hand, robust matrix solution approaches have been adopted. In PARACHUTES two type of algebraic solvers are available: an iterative BiCG solver, which allows obtaining a fast solution with minimum memory requirements; and two more robust direct approaches based on LU factorization and matrix equilibration. In addition, in order to take the most of these approaches, the code can switch automatically between them if required. This allows to speed-up the computations when the system behavior changes little in time (quasi-stationary states) because the solution can be obtained from the previous one with a few iterations of the BiCG solver. If the convergence of the latter fails, the system switches automatically to the direct solver in order to guarantee the accuracy of the solution.

Concerning the problems occurring when computing the loads on the aerodynamic panels (particularly of the canopy), a method to smooth and differentiate variables with safe panel adjacencies is implemented in PARACHUTES. The procedure, based on the undeformed

original geometry and surface curvature criteria, provides control when differentiating across large surface wrinkles, distorted panels and discontinuities such as the trailing edges. Although this is enough to guarantee a satisfactory behavior in most of the cases, additional controls are also implemented to avoid passing to the structure anomalous pressure loads.

The controls outlined above have demonstrated to increase considerably the robustness of the computations with only a slight computational cost (although memory requirements can vary considerably according the algebraic solver used). Currently, additional work is being carried out to achieve further control over instabilities, especially regarding the intersection of body and body-wake panels.

3.3 The coupling methodology

A simple two-way coupling scheme is adopted in PARACHUTES between the aerodynamic (A) and structural (S) solvers. The calculation modules are sequentially advanced in time, exchanging data at the end of each time step. As both solvers are unsteady, the transient dynamic response of the parachute as well as steady-state conditions can be obtained. The transfer of data between the solvers is straightforward because the A and S models share the same mesh. The aerodynamic mesh may contain quadrilateral and/or triangular panels. When a quadrilateral element is passed to the structural solver, it is internally split into a pair of triangles in order to carry out the analysis. As the stability limit of the explicit structural solver is small (due to its explicit character), several structural time increments are performed for each aerodynamic time step.

Due to the fact that the aerodynamic loads are not updated at every step, the high frequency response of the structure can be not well captured. This is not a serious limitation in typical design tasks because high frequency modes have low amplitude, and affect only small parts of the structure. Parachute designers are usually interested in the overall response, where the effect of the low frequency modes is dominant. These modes are well resolved using the simple coupling scheme adopted.

In those cases where only a steady-state solution is sought, convergence can be accelerated by using under-relaxation when updating the forces applied on the structure. This reduces the amount by which the canopy overshoots the equilibrium position during the time-marching procedure and contributes to damp the oscillations faster. Let f^{i-1} be the aerodynamic force applied on a panel at the beginning of a time step i and f^{trial} the force computed on the same panel at the end of the time step. The under-relaxation is achieved by partially updating the force according to

$$f_i = f_{i-1} + \theta(f_i^{\text{trial}} - f_{i-1}) \quad \text{where } 0 < \theta < 1 \quad (98)$$

Satisfactory results are usually obtained by setting $\theta \approx 0.8 - 0.9$ (further details are given in the Program User's Manual [16]).

3.3.1 Apparent-mass effects

For large parachutes the effect of added or apparent mass could be important in transient simulations, see for instance [20]. Thus, to obtain a correct solution in such cases, it would be necessary to account for the inertia of the air surrounding the canopy when computing the mass matrix (in the most extreme cases this problem could even trigger instability in the coupling algorithm). In PARACHUTES, the added-mass model corresponding to Lissaman and Brown [7] has been implemented to calculate the total apparent mass of air surrounding the parachute. Then, this total air mass is distributed between the structural nodes in proportion to its actual nodal mass. This only modifies the structural behavior of the parachute; the effects of apparent mass in the aerodynamics are already accounted for by the unsteady terms involved in the load computation (see Eq. (93)).

3.4 Computational performance

The computational performance of PARACHUTES is under constant improvement. Recently, a considerable part of the code (which is written in FORTRAN 90-95) has been rewritten to increase modularity (and thus simplify the implementation of new features), and to achieve a better computational performance and lower memory requirements. In addition, most of the expensive operations of the aerodynamic solver (e.g. the computation of the influence coefficients) have been parallelized in order to profit from the architecture of current hardware platforms. Note that as the model geometry is changing continuously in time, the global coefficients matrix must be re-computed at each step and the cost involved is considerable.

The parallel performance obtained so far in desktop computers with a small number of cores has been satisfactory, although further testing is required with larger models. The speed-up obtained in parts of the code requiring extensive CPU work, such as the computation of the aerodynamic coefficients, are almost linear. In other parts of the code, involving for instance typical vector operations, the performance gain observed is lower; probably due to the fact that the parallel overhead and cache misses are considerable in relation to the low cost of the computations performed (the typical aerodynamic models employed are not large enough to note a large impact in these operations). At present, further work is being done to improve the computational performance of the code and to complete its parallelization. In addition, tests on

higher performance hardware platforms are to be done in the near future to determine the performance of PARACHUTES when large problems are undertaken. Details of the computational cost involved in typical parachute simulations (mainly memory and CPU-times) are given in the Program User's Manual [16].

4 PARACHUTES graphical user interface

A user interface for the PARACHUTES program has been implemented using the GiD pre- and post-processing software [21]. The user interface allows configuring the solver input parameters and facilitates the use and evaluation of the code, maintaining most of the functional features included in its research version. With this interface, the user can also profit from all the tools available in GiD for importing, creation and reparation of geometry, mesh generation and visualization and analysis of the numerical results. A detailed description of the graphical interface and application tutorials demonstrating the usage of PARACHUTES are presented in the Program User's Manual [16].

5 Conclusions

The theoretical formulation and numerical implementation used in PARACHUTES have been described in this document. The simulation software is under development and several improvements and validation tasks are currently under way. The present work is mainly focused on enhancing modelling capabilities and computational performance (CPU-time and memory requirements). Furthermore, some improvements intended to increase the robustness of the simulations are also carried out. The increase of the modularity (to facilitate future developments) and the easiness of utilization are also important short-term objectives in the development of PARACHUTES.

References

1. PARACIMSA. *New simulation tools for parachute design improvements*. REF. CIT-020400-2005-30. Programa PROFIT, Ministerio de Educación y Ciencia, 01/01/2005 - 31/12/2005.
2. PARAPLANE. *Development of a New Steerable Parachute System for Rescue of Small and Medium Size Airplanes*. REF. 315105-. Seventh Framework Program, European Comission, 01/12/2012 - 30/06/2015.
3. PARAPLANE. Web page: <http://www.cimne.com/paraplane>, CIMNE 2014.
4. CIMSA Ingeniería en Sistemas. Web page: <http://www.cimsa.com/> (October 2014).
5. Ashby, D.L., *Potential flow theory and operation guide for the panel code PMARC_14*. NASA TM-1999-209582, 1999.

6. Maskew, B., *Program VSAERO theory document. A computer program for calculating nonlinear aerodynamic characteristics of arbitrary configurations*. NASA Report 4023, 1987.
7. Lissaman, P., Brown, G., *Apparent mass effects on parafoil dynamics*. AIAA Paper 1993-1236, 1993: p. 10-13.
8. Ortega, E., R. Flores, and E. Oñate, *A 3D low-order panel method for unsteady aerodynamic problems*. CIMNE publication PI 343, 2010.
9. Flores, R., E. Ortega, and E. Oñate, *Explicit dynamic analysis of thin membrane structures*. CIMNE publication PI 351, 2010.
10. Flores, R., Ortega, E., Onate, E., *Simple and efficient numerical tools for the analysis of parachutes*. Engineering Computations, 2014. **31**(5).
11. Zienkiewicz, O.C., R.L. Taylor, and J.Z. Zhu, *The finite element method: Its basis and fundamentals*. Vol. 1. 2005: Butterworth-Heinemann.
12. Hughes, T.J.R., *The finite element method: Linear static and dynamic finite element analysis*1987: Prentice-Hall.
13. Belytschko, T., W.K. Liu, and B. Moran, *Nonlinear finite elements for continua and structures*2000: John Wiley & Sons.
14. Taylor, R.L., *Finite element analysis of membrane structures*. CIMNE publication, 2001.
15. Rossi, R., *A finite element formulation for 3D membrane structures including a wrinkling modified material model*. CIMNE Publication 226, 2003.
16. De la Torre, D., E. Ortega, and R. Flores, *PARACHUTES. A computer program for calculating ram-air parachutes. User's manual*. CIMNE publication, 2015.
17. Cicolani, L., Kanning, G., *A comprehensive estimate of the static aerodynamic forces and moments of the 8- by 8- by 20-Foot cargo container*. NASA Technical Memorandum 89433, 1987.
18. Greenwell, D.I., *Modelling of static aerodynamics of helicopter underslung loads*. Aeronautical Journal, 2011. **115**(1166): p. 201-219.
19. Katz, J. and A. Plotkin, *Low-Speed aerodynamics. From wing theory to panel methods*.1991: McGraw-Hill.
20. Cockrell, D.J., *The aerodynamics of parachutes*. AGARDograph N° 295. AGARD-AG-295, 1987.
21. GiD. *The personal pre and post processor*. Web page: <http://www.gidhome.com>, CIMNE 2014.